Influence of the $SmCo_5$ hard magnetic phase on the magnetoresistive properties of Cu–Fe ribbons

2004 J. Phys.: Condens. Matter 16 7477

(http://iopscience.iop.org/0953-8984/16/41/026)

INSTITUTE OF PHYSICS PUBLISHING JOURNAL OF PHYSICS: CONDENSED MATTER

J. Phys.: Condens. Matter **16** (2004) 7477–7492 PII: S0953-8984(04)81268-2

Influence of the $SmCo_5$ hard magnetic phase on the magnetoresistive properties of Cu–Fe ribbons

R Lardé[1], J M Le Breton[1], F Richomme[1], J Teillet[1], A Hauet[1], A Maignan[2] and O Crisan[3]

[1] Groupe de Physique des Matériaux UMR CNRS 6634, Université de Rouen, Avenue de l'université BP 12, 76801 St Etienne du Rouvray cedex, France
[2] Laboratoire CRISMAT-UMR 6508, ISMRA, 6 boulevard du Maréchal Juin, F-14050 CAEN cedex, France
[3] National Institute for Materials Physics, PO Box MG-7, 76900 Bucharest, Romania

Received 26 May 2004, in final form 22 July 2004
Published 1 October 2004
Online at stacks.iop.org/JPhysCM/16/7477
doi:10.1088/0953-8984/16/41/026

Abstract

The $SmCo_5$ hard magnetic phase was added to magnetoresistive granular Cu–Fe alloys in order to investigate the influence of the presence of a hard magnetic phase on the magnetoresistive properties of a granular alloy that contains a soft magnetic phase. $Cu_{80}(Sm_{0.17}Co_{0.83})_xFe_{20-x}$ ribbons, with $x = 20, 15, 10, 5$, obtained by melt spinning, were investigated. The ribbons are composed of magnetic Fe, $SmCo_5$, and Co precipitates embedded in a Cu matrix. In the as-quenched state, the magnetic interactions between magnetic precipitates lead to the formation of magnetic coherent regions and the magnetoresistance effect is only observed at high field (>1 T). After annealing, the strength of interactions decreases and a magnetoresistance effect is observed at low field (<1 T). The largest magnetoresistance effect (16%) is observed at 5 K for the $Cu_{80}(Sm_{0.17}Co_{0.83})_{10}Fe_{10}$ alloy annealed at 450 °C.

1. Introduction

The phenomenon of giant magnetoresistance (GMR) was first discovered in 1988 in magnetic Fe/Cr multilayers [1]. It was later observed, in 1992, in granular heterogeneous alloys [2, 3]. These alloys are composed of nanosized precipitates of a magnetic metal (Fe, Co), dispersed in a non-magnetic metallic matrix (Ag, Cu). The great interest in such materials is based on the possibility of their use in magnetoresistive heads or magnetic sensors. GMR in granular systems is of the same origin as in magnetic layers, that is, spin dependent scattering of electrons either within or at the interfaces of magnetic precipitates embedded in the non-magnetic matrix. The important role of layer thickness in magnetic multilayers is for granular systems replaced by magnetic precipitate size and inter-precipitate distance. These systems are cheaper and very easy to produce and their microstructure can be modified by suitable heat treatments.

Granular systems are commonly prepared by sputtering or coevaporation of immiscible magnetic and non-magnetic metals. Other non-equilibrium preparation methods, such as melt spinning and mechanical alloying, have also been used. The major problem of these granular systems is the high magnetic field H_S required for saturation of the magnetization, due to the presence of superparamagnetic precipitates, giving a ratio MR/H (MR sensitivity) too small for applications. In order to characterize the effect of the presence of a hard magnetic phase on the magnetoresistive properties the $SmCo_5$ phase was added to Cu–Fe granular alloys. Such a system is composed of several magnetic phases and exhibits a complex magnetic nanostructure with magnetic coupling among the nanograins [4]. Therefore one may expect a characteristic magnetoresistive behaviour. It is clear that the addition of the $SmCo_5$ hard magnetic phase in Cu–Fe granular alloys could lead to a reduction of the maximal MR amplitude due to the enhancement of the magnetic coupling between magnetic precipitates. However, such an addition could reduce the saturation magnetic field H_S by blocking the superparamagnetic precipitates.

In this paper, the influence of both microstructure and interactions among the magnetic precipitates on the magnetoresistive properties of $Cu_{80}(Sm_{0.17}Co_{0.83})_xFe_{20-x}$ ribbons ($x = 20, 15, 10, 5$) is investigated.

2. Experimental procedure

The $Cu_{80}(Sm_{0.17}Co_{0.83})_xFe_{20-x}$ ($x = 20, 15, 10, 5$) alloys were obtained using a single-roller melt-spinning method, with a 40 cm diameter Cu roller, and a 30 m s^{-1} speed corresponding to a 10^6 K min^{-1} cooling rate. The initial constituents used to form the initial molten alloy are Cu, Fe, and $SmCo_5$. The ribbons obtained from the liquid quenching have a thickness of about 15–20 μm and a width of about 2–3 mm. The resulting as-quenched samples were annealed at 400, 450, 520, and 650 °C for 1 h. The heat treatments were performed in a resistive furnace, under ultrahigh vacuum (10^{-7} bar). The structural analysis of untreated and treated samples was performed by x-ray diffraction, Mössbauer spectrometry, and transmission electron microscopy. The XRD analyses were carried out with a fast curved detector (INEL CPS 120) using the Co Kα radiation ($\lambda = 0.179\,02$ nm). Transmission ^{57}Fe Mössbauer spectrometry was performed at room temperature with a conventional spectrometer using a ^{57}Co source in a rhodium matrix. The TEM analyses were performed using a JEOL 2000FX microscope. The magnetic properties were investigated from zero-field-cooled (ZFC) and field-cooled (FC) curves, and hysteresis loops. The magnetic data were obtained using a Quantum Design MPMS*XL* SQUID magnetometer. The magnetic field was applied parallel to the ribbon plane. The electrical resistivity and magnetoresistive measurements were performed at room temperature and at 5 K using the four-probe method with a Quantum Design PPMS, under a magnetic field up to 7 T, applied parallel to the ribbon plane. The MR ratio was defined as usual as $([R(H) - R(H = 0)]/R(H = 0)) \times 100$.

3. Structural characterization

3.1. X-ray diffraction

The XRD patterns of the as-quenched $Cu_{80}(Sm_{0.17}Co_{0.83})_xFe_{20-x}$ samples (figure 1) show for all x values the presence of three crystalline phases: Cu (fcc), α-Fe (bcc), and $SmCo_5$ (hcp). For $x = 15$ and 20, the peaks of the β-Co phase are observed. As x increases, the intensity of the $SmCo_5$ peaks increases while that of the α-Fe peaks decreases. This evolution is in agreement with the increasing $SmCo_5$ content and the decreasing α-Fe content.

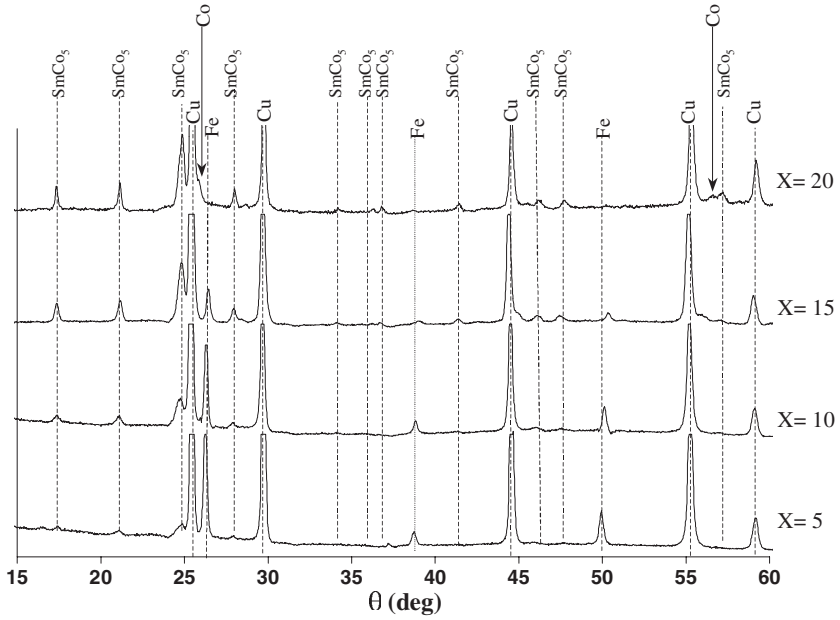

Figure 1. X-ray diffraction patterns of the as-quenched $Cu_{80}(Sm_{0.17}Co_{0.83})_xFe_{20-x}$ ribbons.

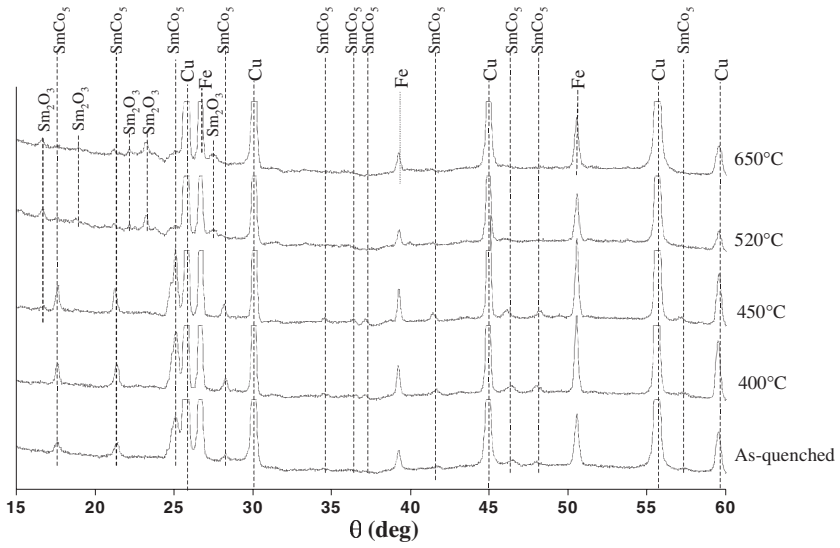

Figure 2. X-ray diffraction patterns of the as-quenched and annealed $Cu_{80}(Sm_{0.17}Co_{0.83})_{10}Fe_{10}$ ribbons.

The structural evolution of the ribbons during the annealing treatment was followed for each composition. In figure 2 we show the evolution of the XRD pattern of the $Cu_{80}(Sm_{0.17}Co_{0.83})_{10}Fe_{10}$ ribbons as a function of the annealing temperature. Up to 450 °C the $SmCo_5$ peaks are refined and their intensity increases. Above 450 °C, the $SmCo_5$ peaks disappear and several peaks of the oxide phase Sm_2O_3 are observed. The same evolution is observed for the $Cu_{80}(Sm_{0.17}Co_{0.83})_5Fe_{15}$ ribbons.

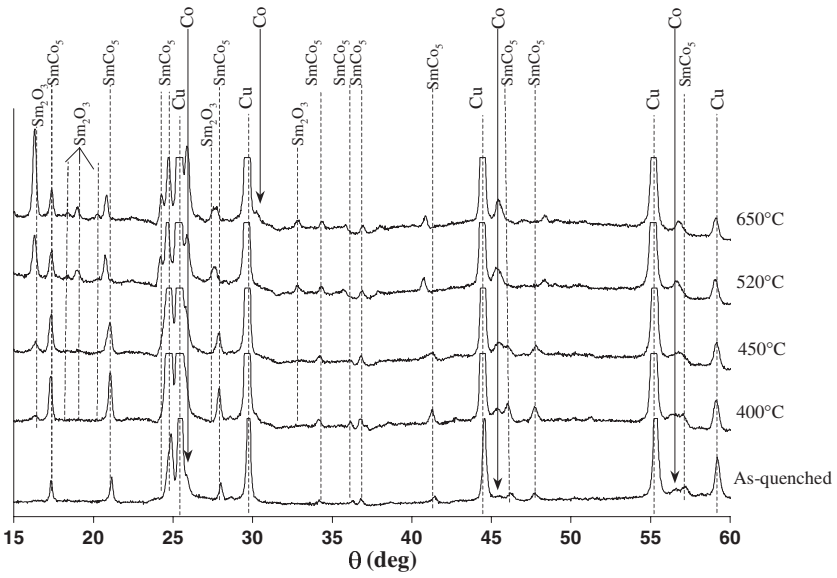

Figure 3. X-ray diffraction patterns of the as-quenched and the annealed $Cu_{80}(Sm_{0.17}Co_{0.83})_{20}$ ribbons.

For a higher $SmCo_5$ content ($x = 15, 20$), the structural evolutions of the different samples are similar. This is shown for the $x = 20$ sample in figure 3, where the $SmCo_5$ peaks are well defined and are refined upon annealing. At 400 °C, Sm_2O_3 peaks appear and their intensity increases with the annealing temperature. The formation of Sm_2O_3 is attributed to the oxidation of the $SmCo_5$ phase and is correlated with the appearance of the β-Co peaks. Upon annealing, the intensity of the β-Co peaks increases, corresponding to the precipitation of Co precipitates, related to the oxidation of Sm.

These results show that the ribbons are composed of several crystalline phases: Cu, α-Fe, $SmCo_5$, and β-Co for higher $SmCo_5$ concentration. The phase separation in the alloy may have occurred either during the quenching process or prior to quenching when the alloy existed in the liquid phase. According to the Fe–Cu phase diagram, Cu and Fe are miscible in the liquid phase. Therefore the phase separation of Fe and Cu occurred during the quenching process. Moreover, if the alloy in the liquid phase had been homogeneous, Sm–(Co, Fe, Cu) phases would have been formed during quenching. Here, only the $SmCo_5$ phase is observed, indicating that the phase separation of Cu and $SmCo_5$ occurred prior to quenching. Up to 450 °C, the annealing treatment leads to a structural refinement but increasing the annealing temperature above 450 °C causes the oxidation of Sm. For a high $SmCo_5$ content ($x = 15, 20$) this oxidation is correlated with the precipitation of the β-Co phase. The stable Co phase (hcp) is not observed and the presence of the fcc structure can be explained by the presence very small Co precipitates, crystallographically coherent with the Cu matrix.

3.2. Mössbauer analyses

For the whole series of Fe containing samples, the Mössbauer spectra consist of a magnetic contribution attributed to Fe atoms in a magnetic environment (α-Fe), and a central component corresponding to Fe atoms in a paramagnetic environment (see figure 4 for $x = 10$). The magnetic contribution was fitted with a distribution of sextets. The central component was fitted with two or three doublets and one singlet, depending on the spectrum.

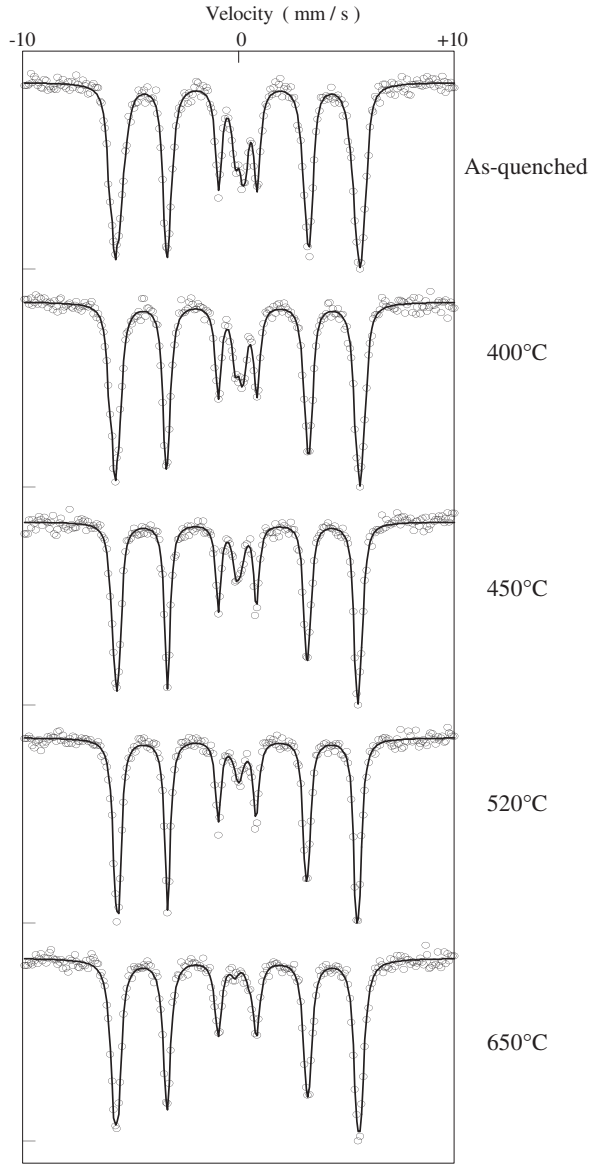

Figure 4. Mössbauer spectra of the as-quenched and annealed $Cu_{80}(Sm_{0.17}Co_{0.83})_{10}Fe_{10}$ ribbons.

The results show that in the as-quenched ribbons with $x = 5$, 10, and 15, about 85% of the Fe atoms are present in a magnetic environment. For $x = 5$ and 10 the values obtained for the hyperfine field (36.0 and 34.9 T respectively) are higher than 33 T, indicating that Co atoms are present in the α-Fe phase. For $x = 15$ the value of the hyperfine field (32.5 T) is lower than 33 T, indicating the presence of Cu atoms in the α-Fe phase. The remaining 15% of the Fe atoms are present in non-magnetic environments related to the Fe–Cu phase, in α-Fe superparamagnetic nanosized precipitates, or in the γ-Fe phase [5].

For the whole series of samples the evolutions of the Mössbauer spectra are approximately the same. In figure 4 we report the room temperature Mössbauer spectra of the $Cu_{80}(Sm_{0.17}Co_{0.83})_{10}Fe_{10}$ ribbons, as-quenched and annealed for 1 h at 400, 450, 520,

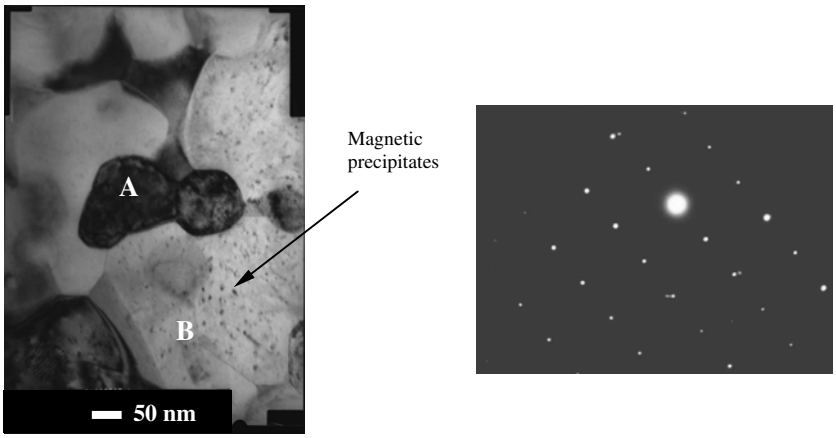

Figure 5. (a) A TEM micrograph of the $Cu_{80}(Sm_{0.17}Co_{0.83})_{10}Fe_{10}$ ribbons annealed at 450 °C. The dark zones (A) represent the Cu grains containing about 70% Cu and the bright zones (B) represent the Cu grains containing 95% Cu. (b) A diffraction pattern of the hexagonal $SmCo_5$ phase obtained in a dark zone.

and 650 °C. On increasing the annealing temperature, the singlet disappears and the intensity of the central component decreases. After annealing at 650 °C, only 2–3% of Fe atoms remain in a paramagnetic environment. For the samples with $x = 5$ and 10, the value of the mean hyperfine field increases up to 37 T upon annealing. This indicates that the proportion of Co atoms in the α-Fe(Co) phase increases. After annealing at 650 °C, the proportion of Co in α-Fe, estimated from the value of the mean hyperfine field, ranges between 22% and 30% [6]. For lower Fe content ($x = 15$), the mean hyperfine increases up to 33.3 T upon annealing. The estimated corresponding proportion of Co atoms in the α-Fe phase is 2–4%, much lower than in annealed $x = 5$ and 10 samples. This result is correlated with the precipitation of the β-Co phase in the $x = 15$ and 20 samples, as observed by XRD.

The Mössbauer analyses show that for all the Fe containing samples a majority of Fe atoms are present in the α-Fe(Co) phase. However, in the as-quenched state 15% of Fe atoms are present in paramagnetic environment, corresponding to an Fe–Cu phase, Fe superparamagnetic precipitates, or γ-Fe phase. The heat treatments lead to a decrease of the fraction of the paramagnetic component, attributed both to the Cu phase purification by segregation of Fe atoms, and to the growth of initially superparamagnetic Fe precipitates. For an Fe content of 10% or more, an increase of the Co content in the α-Fe(Co) phase upon annealing was observed, related to the oxidation of the $SmCo_5$ phase observed by means of XRD. For an Fe content lower than 10%, the proportion of Co atoms in the α-Fe phase is weak (about 2–4%); this is related to the precipitation of the β-Co phase observed by XRD.

Moreover, the Mössbauer analyses show that Fe atoms are not present in the $SmCo_5$ phase whereas some Fe atoms are dissolved in the Cu matrix. This observation confirms that before quenching, the alloy in the liquid phase was not homogeneous, being composed of $SmCo_5$ globules embedded in the Cu–Fe phase.

3.3. TEM analyses

The $Cu_{80}(Sm_{0.17}Co_{0.83})_{10}Fe_{10}$ and $Cu_{80}(Sm_{0.17}Co_{0.83})_{20}$ ribbons annealed at 450 °C were investigated by TEM. A bright field image of the $Cu_{80}(Sm_{0.17}Co_{0.83})_{10}Fe_{10}$ ribbon is shown in figure 5. Dark (A) and bright (B) zones are observed. The EDX analyses show that the

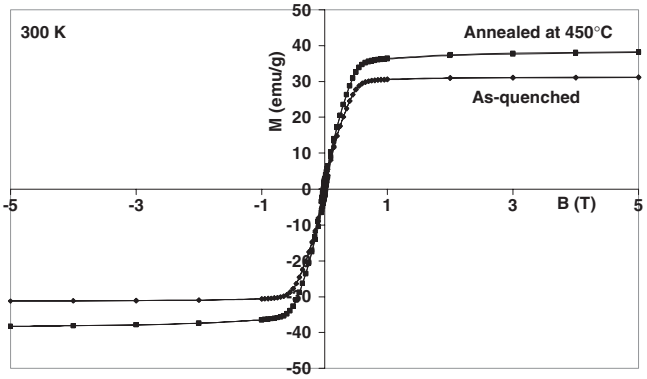

Figure 6. The magnetization (emu g^{-1}) of $Cu_{80}(Sm_{0.17}Co_{0.83})_{10}Fe_{10}$ ribbons, as-quenched and annealed for 1 h at 450 °C, as a function of the magnetic field (T).

dark zones (A) are composed of Cu grains (70%), containing 18% Fe, 8% Co, and 4% Sm. The bright zones (B) are composed of Cu rich grains (95%) containing a small fraction of Fe, Sm, and Co atoms. The mean size of all the Cu grains is about 150 nm. Moreover, nanosized precipitates (<10 nm) are observed in the Cu grains, which may correspond to the α-Fe and $SmCo_5$ precipitates detected by means of XRD. These results show that the $Cu_{80}(Sm_{0.17}Co_{0.83})_{10}Fe_{10}$ ribbon is composed of two classes of Cu grains. The results of the TEM investigation of the $Cu_{80}(Sm_{0.17}Co_{0.83})_{20}$ ribbons are similar. Two classes of Cu grains are also observed. The first class contains 90 at.% of Cu and 10 at.% of Co and the second contains 60 at.% of Cu and 36 at.% of Co and 4 at.% Sm.

These results confirm that $Cu_{80}(Sm_{0.17}Co_{0.83})_xFe_{20-x}$ ribbons are composed of nanosized magnetic precipitates embedded in the Cu matrix. The dispersion of these precipitates is not homogeneous and some Cu grains are rich in magnetic precipitates while the others contains a few magnetic elements.

4. Magnetic and transport properties

4.1. Magnetic measurements

The hysteresis loops obtained at 300 K for the as-quenched $Cu_{80}(Sm_{0.17}Co_{0.83})_{10}Fe_{10}$ and $Cu_{80}(Sm_{0.17}Co_{0.83})_{20}$ ribbons (figures 6 and 7) are characterized by a rapid saturation at low magnetic field. The coercivities of the as-quenched $Cu_{80}(Sm_{0.17}Co_{0.83})_{10}Fe_{10}$ and $Cu_{80}(Sm_{0.17}Co_{0.83})_{20}$ ribbons are 200 and 400 Oe, respectively.

After annealing at 450 °C, the magnetization curves present a steep increase of magnetization at low field followed by a small slope under high magnetic field. This behaviour is due to superparamagnetic contributions attributed to small magnetic precipitates. At 5 K, the magnetization reaches, under 5 T, 39 ± 2 and 23 ± 1 emu g^{-1} for the $Cu_{80}(Sm_{0.17}Co_{0.83})_{10}Fe_{10}$ and $Cu_{80}(Sm_{0.17}Co_{0.83})_{20}$ ribbons, respectively. The corresponding theoretical saturation magnetizations (M_S) are estimated from the nominal compositions according to the following formula: $M_S = X_{Fe} \cdot M_S^{Fe} + X_{SmCo_5} \cdot M_S^{SmCo_5}$, where X_{Fe} and X_{SmCo_5} are the nominal Fe and $SmCo_5$ contents (wt%) and M_S^{Fe} and $M_S^{SmCo_5}$ are the saturation magnetization of pure Fe and pure $SmCo_5$, respectively. The values obtained for the two ribbons are 31 and 22.6 emu g^{-1}, respectively. Comparison of the estimated M_S values with the experimental values shows that the $SmCo_5$ phase contributes to the magnetization of $Cu_{80}(Sm_{0.17}Co_{0.83})_xFe_{20-x}$ ribbons and

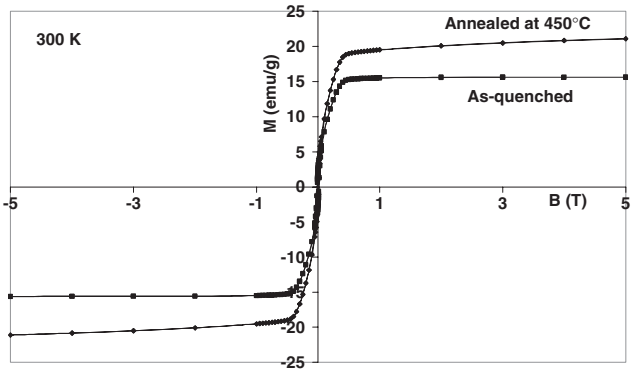

Figure 7. The magnetization (emu g^{-1}) of $Cu_{80}(Sm_{0.17}Co_{0.83})_{20}$ ribbons, as-quenched and annealed for 1 h at 450 °C, as a function of the magnetic field (T).

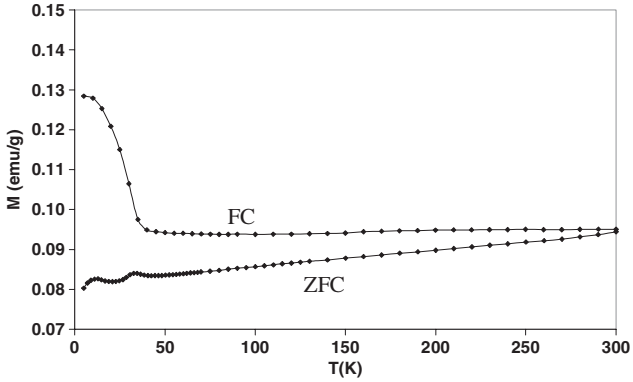

Figure 8. ZFC/FC curves of the as-quenched $Cu_{80}(Sm_{0.17}Co_{0.83})_{10}Fe_{10}$ ribbon ($H = 30$ Oe).

the low coercivity suggests that the magnetic moments of the $SmCo_5$ precipitates are easily aligned towards the magnetic field during the magnetization process. This result is coherent with the reduction of the coercivity with the $SmCo_5$ precipitate size [7] and confirms that the $SmCo_5$ hard magnetic phase is composed of nanosized precipitates ($\sim$10 nm).

The ZFC/FC curves reported in figures 8–10 reveal a complex magnetic behaviour. The characteristic feature of a ZFC/FC curve is the occurrence of a peak in the ZFC magnetization curve, related to the progressive deblocking on increasing temperature of superparamagnetic precipitates. The FC curves correspond to the blocking of these precipitates on decreasing temperature.

The ZFC curve of the as-quenched $Cu_{80}(Sm_{0.17}Co_{0.83})_{10}Fe_{10}$ ribbon (figure 8) exhibits two small peaks followed by a slight increase of the magnetization. These peaks can be associated with the progressive deblocking of two classes of superparamagnetic precipitates characterized by different size distributions or different magnetic anisotropies. The subsequent slight increase of the magnetization is attributed to the deblocking of a third class of precipitates having a larger size or a higher magnetic anisotropy. After annealing at 450 °C, only one peak is observed in the ZFC curve (figure 9) and the values of the magnetization are higher than that obtained for the corresponding as-quenched ribbon. This suggests than the proportion of the superparamagnetic precipitates is higher after annealing at 450 °C than after quenching.

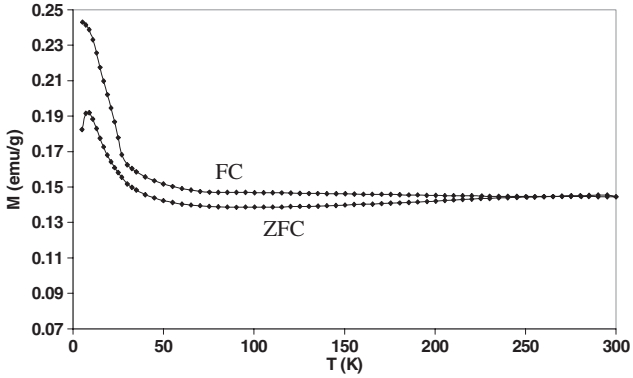

Figure 9. ZFC/FC curves of the $Cu_{80}(Sm_{0.17}Co_{0.83})_{10}Fe_{10}$ ribbon annealed at 450 °C (H = 30 Oe).

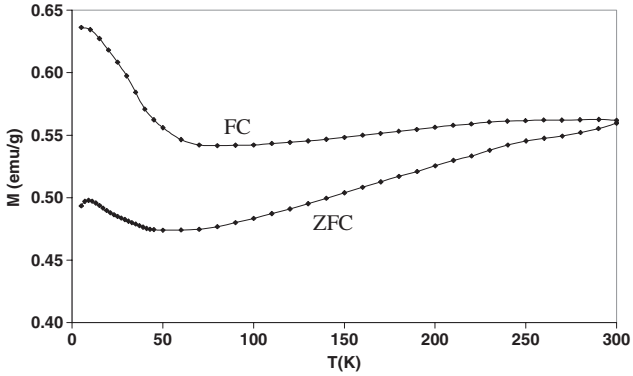

Figure 10. ZFC/FC curves of the $Cu_{80}(Sm_{0.17}Co_{0.83})_{20}$ ribbon annealed at 450 °C (H = 30 Oe).

This result is in agreement with the occurrence of a superparamagnetic contribution observed in the hysteresis loop of the same annealed ribbon (figure 6). The ZFC curve of the annealed $Cu_{80}(Sm_{0.17}Co_{0.83})_{20}$ ribbon is composed of a peak followed by an increase of the magnetization. The values of the magnetization are higher than those obtained for both as-quenched and annealed $Cu_{80}(Sm_{0.17}Co_{0.83})_{10}Fe_{10}$ ribbon suggesting the presence of a more important superparamagnetic contribution. This result is also correlated with the occurrence of a superparamagnetic contribution observed in the hysteresis loop of the same annealed ribbon. According to the results of the structural investigation, we assume, first, that the low temperature peaks observed in the ZFC curves correspond to the deblocking of Fe(Co) and Co superparamagnetic precipitates and, second, that the following increase of the magnetization corresponds to the deblocking of $SmCo_5$ superparamagnetic precipitates.

All the FC curves are characterized by a strong increase of the magnetization below 50 K whereas a soft increase is expected in the case of a progressive blocking of non-interacting superparamagnetic precipitates. This behaviour may be explained by the existence of magnetic interactions between the magnetic entities [8].

4.2. Transport properties

For all samples, a typical variation of the resistance with temperature is observed. As the temperature decreases, the resistance decreases, due to the reduction of electron–phonon

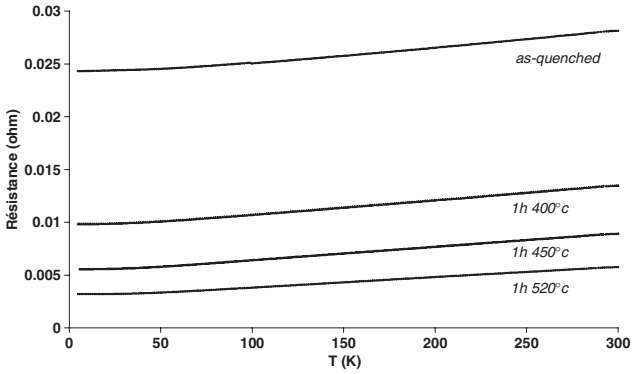

Figure 11. The resistance of $Cu_{80}(Sm_{0.17}Co_{0.83})_{10}Fe_{10}$ as-quenched and annealed ribbons as a function of temperature.

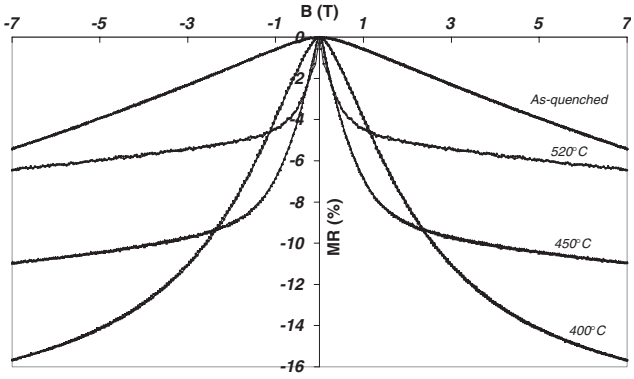

Figure 12. The magnetoresistance at 5 K of the as-quenched and annealed $Cu_{80}(Sm_{0.17}Co_{0.83})_{10}Fe_{10}$ ribbons.

interactions, and then reaches a stable value at low temperature, which corresponds to the residual resistivity. In figure 11 we report the resistance versus temperature curves for the as-quenched and annealed $Cu_{80}(Sm_{0.17}Co_{0.83})_{10}Fe_{10}$ ribbons. After annealing at 400 °C, an important drop of the residual resistance (at 5 K) is observed. This residual resistance decreases upon annealing, and this confirms the purification of the Cu matrix by both strain relaxation and elimination of defects.

Magnetoresistance as a function of the magnetic field has been measured for all the samples at 5 and 300 K. The general expected shape of a magnetoresistance curve consists of two parts corresponding to two regimes: an initial steep decrease followed by a long tail as the magnetic field increases. This initial steep decrease in resistivity is associated with a rapid rise of the magnetization due to the rotation of the magnetization of the magnetic precipitates towards the applied field. This contribution to the MR is similar to the spin-valve MR observed in magnetic multilayers and has been termed a 'spin-valve' contribution [6]. The long MR tail at high magnetic field corresponds to a very small change in the magnetization of the sample as it approaches saturation. This behaviour of MR in high field regions is due to the progressive decrease in the scattering caused by magnetic disorder, for instance paramagnetic or superparamagnetic fluctuations.

Figure 12 shows the evolution upon annealing of the magnetoresistance curves of the $Cu_{80}(Sm_{0.17}Co_{0.83})_{10}Fe_{10}$ ribbon. The magnetoresistance of the as-quenched ribbon varies

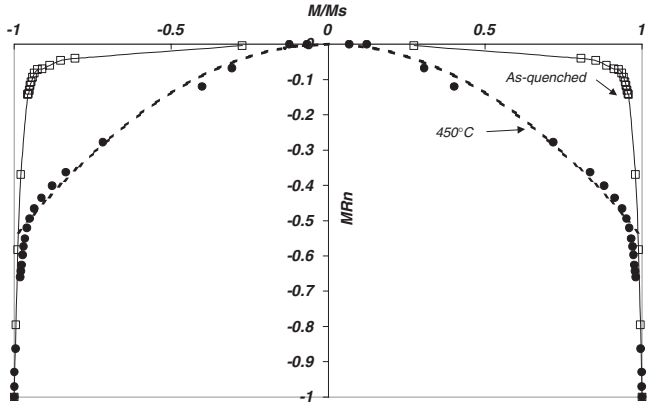

Figure 13. The normalized magnetoresistance (MR_n) of as-quenched and annealed $Cu_{80}(Sm_{0.17}Co_{0.83})_{10}Fe_{10}$ ribbons at 5 K, as a function of the normalized magnetization (M/M_S).

linearly with the magnetic field and reaches 5.5% at 7 T. No saturation is observed. A similar behaviour is observed for the other as-quenched ribbons. After annealing at 400 °C the 'spin-valve' contribution appears and the amplitude of MR reaches 16% at 7 T. It is the maximum MR value obtained over the whole series of ribbons. After annealing at 450 °C, the sensitivity of MR in low magnetic field is improved and reaches its optimum whereas the MR tail at higher field shows a tendency towards saturation. Above 450 °C, the 'spin-valve' contribution decreases and the magnetoresistance progressively vanishes. This evolution of the magnetoresistance curves with the annealing temperature can be explained by microstructural changes in the ribbon during annealing, as the annealing induces an evolution of both the size of the magnetic precipitates and their distribution within the Cu matrix.

The normalized magnetoresistance ($MR_n = MR(H)/MR(5\ T)$) obtained at 5 K for the $Cu_{80}(Sm_{0.17}Co_{0.83})_{10}Fe_{10}$ ribbon, both as-quenched and annealed at 450 °C, is represented as a function of the reduced magnetization in figure 13. For an assembly of non-interacting superparamagnetic precipitates, the magnetoresistance ratio is related to the square of the reduced magnetization ($MR_n \propto (M/M_S)^2$) and a parabolic behaviour is expected.

In the as-quenched state, such a behaviour is not observed and the curve exhibits a box-like shape. This curve shows that the largest magnetoresistance effect is observed above $M/M_S = 0.9$ and corresponds to very slight changes in the magnetization. The deviation from the predicted parabolic behaviour has already been observed in numerous studies [9–13]. This deviation can be explained by taking into account magnetic interactions [10, 11] and by considering the particle size distribution [12–15]. In general this deviation leads to a flat top parabola. Curves characterized by a box-like shape were observed in Au–Fe and Au–Co systems [16, 17]. In these systems, this behaviour is explained by the existence of adjacent magnetic regions (due to interactions between magnetic moments of diluted magnetic atoms) characterized by a magnetic coherence length. In our ribbons, magnetic interactions between magnetic precipitates may lead to the occurrence of magnetic coherent regions composed of several magnetic precipitates. Within each region, a certain degree of misalignment of magnetic moments of precipitates exists (figure 14(a)). Thus the initial steep increase of magnetization observed in the hysteresis loop at low field may be due to the reorientation towards the magnetic field of the global magnetization of the magnetic coherent regions. This reorientation seems to have a very slight effect on the magnetoresistance because of the large magnetic coherence length. The slight changes in the magnetization at high field are related to the alignment of the

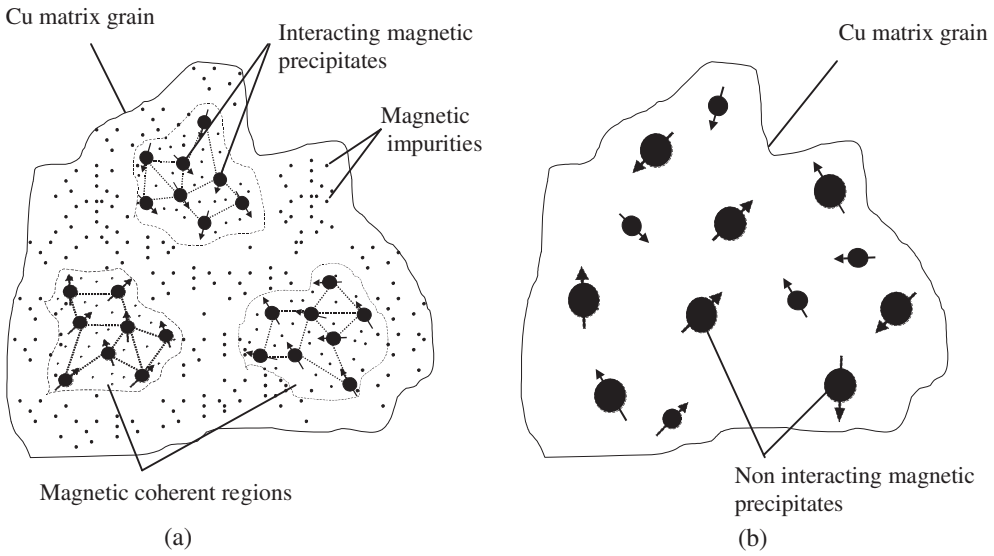

Figure 14. Schematic magnetic structure of (a) as-quenched and (b) annealed $(Sm_{0.17}Co_{0.83})_xFe_{20-x}$ ribbons. In the as-quenched state (a), magnetic impurities and magnetic precipitates are dispersed in the Cu matrix. Interactions between the magnetic precipitates lead to the formation of coherent magnetic regions. After annealing (b), the magnetic precipitates coarsen and the matrix is purified leading to the formation of new superparamagnetic precipitates. The interactions between the precipitates disappear.

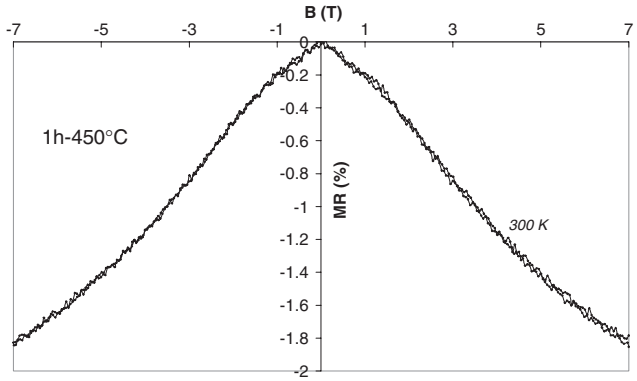

Figure 15. The magnetoresistance at 300 K of the $Cu_{80}(Sm_{0.17}Co_{0.83})_{10}Fe_{10}$ ribbon annealed at 450 °C.

canting moment of magnetic precipitates along the magnetic field and give rise to the largest magnetoresistance effect observed above $M/M_S > 0.9$.

After annealing at 450 °C, the MR_n curve presents two distinct regions: the first region ($M/M_S < 0.9$) shows a parabolic behaviour (figure 13, dashed line); the second region ($M/M_S > 0.9$) shows the same behaviour as in the as-quenched state. The appearance of a parabolic behaviour is correlated with the appearance of the 'spin-valve contribution'. This suggests a decrease of the interaction strength and disappearance of the coherent regions (figure 14(b)).

At 300 K, the magnetoresistance of the $Cu_{80}(Sm_{0.17}Co_{0.83})_{10}Fe_{10}$ ribbon annealed at 450 °C is decreased and reaches about 1.8% at 7 T (figure 15). The corresponding normalized

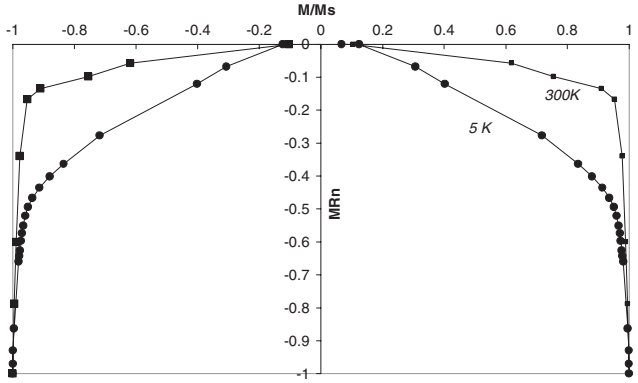

Figure 16. The normalized magnetoresistance (MR_n) at 5 and 300 K of the $Cu_{80}(Sm_{0.17}Co_{0.83})_{10}Fe_{10}$ ribbon annealed at 450 °C as a function of the normalized magnetization (M/M_S).

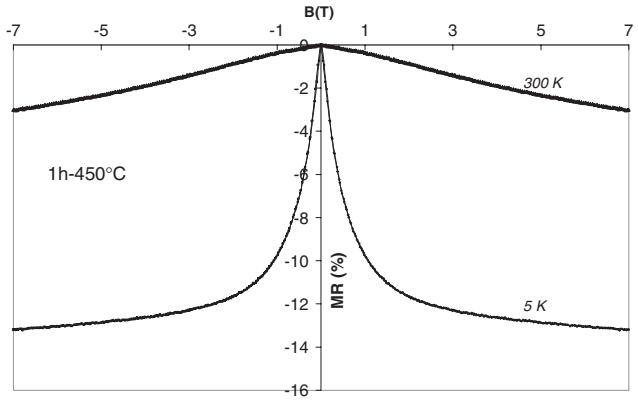

Figure 17. The magnetoresistance at 5 and 300 K of the $Cu_{80}(Sm_{0.17}Co_{0.83})_{15}Fe_5$ ribbon annealed at 450 °C.

magnetoresistance as a function of the normalized magnetization is reported in figure 16. The curve exhibits a box-like shape while at 5 K a region with parabolic behaviour was observed. The disappearance of this parabolic region at 300 K is related to the deblocking of the superparamagnetic precipitates responsible for the 'spin-valve contribution' at 5 K. This deblocking is observed in the ZFC/FC curves and it corresponds to the small slope in high magnetic field observed at 300 K in the $M(H)$ hysteresis loop (figure 8).

The magnetoresistance curves obtained at 5 and 300 K for the $Cu_{80}(Sm_{0.17}Co_{0.83})_{15}Fe_5$ and $Cu_{80}(Sm_{0.17}Co_{0.83})_{20}$ ribbons annealed at 450 °C are presented in figures 17 and 18 respectively. These curves present the same behaviour as for the $Cu_{80}(Sm_{0.17}Co_{0.83})_{10}Fe_{10}$ ribbon. At 5 K, the magnetoresistance of the $Cu_{80}(Sm_{0.17}Co_{0.83})_{15}Fe_5$ and $Cu_{80}(Sm_{0.17}Co_{0.83})_{20}$ ribbons annealed at 450 °C seems to reach saturation: 13.2% and 11.5%, respectively, at 7 T. The magnetoresistance of the $Cu_{80}(Sm_{0.17}Co_{0.83})_{15}Fe_5$ annealed at 450 °C ribbon presents the best MR sensitivity at low field for the whole series of ribbons. In figure 19 we present the normalized magnetoresistance at 5 and 300 K of the $Cu_{80}(Sm_{0.17}Co_{0.83})_{20}$ ribbon annealed at 450 °C as a function of the normalized magnetization. At 5 K, the box-like shape is not observed. The curve presents instead a parabolic shape. At 300 K, the box-like shape is observed as for the $Cu_{80}(Sm_{0.17}Co_{0.83})_{10}Fe_{10}$ ribbon annealed at 450 °C. At 300 K, the

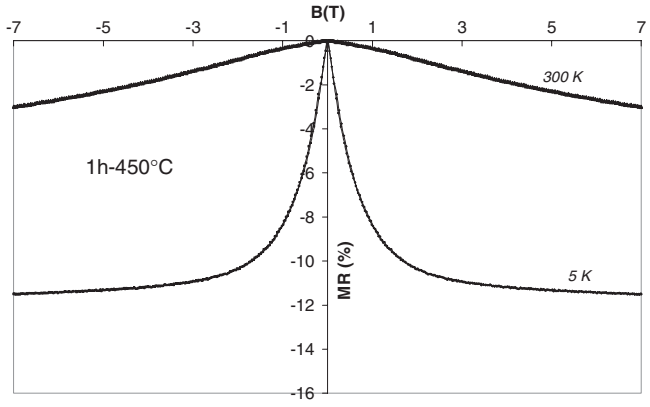

Figure 18. The magnetoresistance at 5 and 300 K of the $Cu_{80}(Sm_{0.17}Co_{0.83})_{20}$ ribbon annealed at 450 °C.

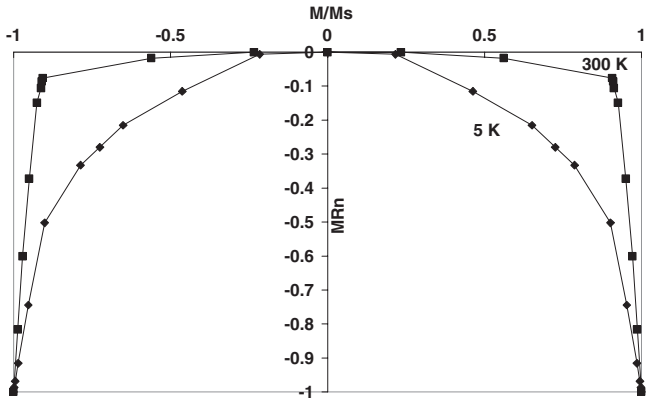

Figure 19. The normalized magnetoresistance (MR_n) at 5 and 300 K for the $Cu_{80}(Sm_{0.17}Co_{0.83})_{20}$ ribbon annealed at 450 °C as a function of the normalized magnetization (M/M_S).

magnetoresistances at 7 T for the $Cu_{80}(Sm_{0.17}Co_{0.83})_{15}Fe_5$ and $Cu_{80}(Sm_{0.17}Co_{0.83})_{20}$ ribbons annealed at 450 °C are approximately the same (3%).

5. Discussion

The above investigations show that in the as-quenched state, all ribbons are composed of interacting magnetic precipitates ($SmCo_5$ and α-Fe, α-Fe(Co), or β-Co) embedded in the Cu matrix. In granular systems composed of magnetic precipitates embedded in a conducting matrix, dipolar and Ruderman–Kittel–Kasuya–Yosida (RKKY) interactions might be expected. These interactions lead to the formation of magnetic coherent regions composed of several adjacent coupled magnetic precipitates. When the samples are magnetized, two regimes are observed. At low field the coherent regions reverse cooperatively, corresponding to the coherent rotation of the magnetic moments of the magnetic precipitates. This coherent rotation leads to an increase of M, but the relative angles between the moments of magnetic precipitates are maintained by the interactions and no magnetoresistance effect is observed. At high magnetic field, the coupling between magnetic precipitates is overcome and magnetic moments

of magnetic precipitates rotate independently, to be aligned along the magnetic field. These reorientations at high field lead to very slight changes of M, but are responsible for the observed magnetoresistance effect in the as-quenched ribbons.

After annealing, a structural evolution of the ribbons is observed. The Cu matrix is purified and the size and the distribution of magnetic precipitates are modified. After annealing at 450 °C, a superparamagnetic contribution appears in the $M(H)$ hysteresis loops recorded at 300 K (figures 6 and 7). The superparamagnetic behaviour of some magnetic precipitates is assumed to be due to the decrease of the magnetic coupling induced by the changes of the size and the distribution of the magnetic precipitates in the Cu matrix. At low temperatures, the blocking of these superparamagnetic precipitates below the blocking temperature leads to the appearance of the 'MR spin-valve' contribution and to the disappearance of the box-like shape of the MR versus M curves. At 300 K, the 'MR spin-valve' contribution is reduced due to the deblocking of the superparamagnetic precipitates, and the shape of the MR versus M curves is near to the box-like shape.

After annealing at 520 °C, magnetic precipitates become too large compared with the mean free path of the conduction electrons and the magnetoresistance effect is reduced. To obtain an optimized magnetoresistance effect, the annealing temperature must range from 400 to 450 °C.

The MR values obtained at 5 K for the optimally annealed $Cu_{80}(Sm_{0.17}Co_{0.83})_xFe_{20-x}$ ribbons (between 10% and 16%) are higher than those observed for Cu–Fe granular systems (<10%) [18–20]. Moreover, the MR sensitivity of the $Cu_{80}(Sm_{0.17}Co_{0.83})_xFe_{20-x}$ ribbons is enhanced compared to that of $Cu_{80}Fe_{20}$ alloys. This seems to indicate that the addition of the $SmCo_5$ hard magnetic phase has a positive effect on the magnetoresistive properties of the $Cu_{80}Fe_{20}$ alloys.

On the other hand, these MR values are comparable to those obtained for Cu–Fe–Co granular alloys (15–20% at 5 K). It is well known that the presence of Co atoms in the Fe precipitates induces an increase of the MR value of $Cu_{80}Fe_{20}$ alloys. In the $Cu_{80}(Sm_{0.17}Co_{0.83})_xFe_{20-x}$ ribbons, Co atoms are present in the Fe precipitates. Thus, the improvement of the magnetoresistive properties of the $Cu_{80}(Sm_{0.17}Co_{0.83})_xFe_{20-x}$ granular ribbons is probably not just due to the presence of the $SmCo_5$ phase, being partly due to the presence of Co atoms in Fe precipitates. It must be added that the $SmCo_5$ phase does not induce a reduction of the MR value, as a significant MR effect is obtained in the $Cu_{80}(Sm_{0.17}Co_{0.83})_xFe_{20-x}$ ribbons with high $SmCo_5$ contents ($x = 15$ and 20).

6. Conclusion

Structural investigations of $Cu_{80}(Sm_{0.17}Co_{0.83})_xFe_{20-x}$ ribbons show that the as-quenched ribbons are composed of several crystalline phases: Cu, α-Fe, and $SmCo_5$. β-Co is present for high $SmCo_5$ concentrations. After quenching, about 12–16% of Fe atoms are dissolved in the Cu matrix. The Mössbauer analyses reveal for $x = 5$ and 10 the presence of Co atoms in the α-Fe phase and for Fe with $x = 15$ the presence of Cu atoms in the α-Fe phase. In the first stages of the annealing treatment a structural refinement is observed corresponding to the strain relaxation and to the phase purification by segregation of Cu, Fe, and Co atoms. Above 450 °C, the annealing causes the oxidation of Sm. For the highest Fe contents (10 and 15%) this oxidation is correlated with the increases of the Co content in the α-Fe phase. For the lowest Fe contents (0 and 5%), this oxidation leads to the precipitation of the β-Co phase.

The investigation of the magnetic and transport properties shows the existence of magnetic interactions among the magnetic precipitates. Considering that a global magnetic moment is associated with each magnetic precipitate, interactions between magnetic precipitates must

lead to the formation of magnetic coherent regions formed by several canted global magnetic moments. These regions give rise to a magnetoresistance effect only at high magnetic field when the magnetic interactions are overcome. After annealing, the interaction strength decreases leading to the disappearance of the coherent regions, and a magnetoresistance effect is observed not only at high field but also at low field.

The results obtained show that granular alloys containing a mixture of hard and soft magnetic phases exhibit a magnetoresistance effect. The largest effect (16% at 7 T) is observed at 5 K for the $Cu_{80}(Sm_{0.17}Co_{0.83})_{10}Fe_{10}$ ribbon annealed at 400 °C, and the best sensitivity at low field is obtained at 5 K for the $Cu_{80}(Sm_{0.17}Co_{0.83})_{15}Fe_5$ ribbon annealed at 450 °C.

The magnetoresistive behaviour of the $Cu_{80}(Sm_{0.17}Co_{0.83})_xFe_{20-x}$ ribbons is very similar to that observed for many heterogeneous alloys. The expected characteristic magnetoresistive behaviour of $Cu_{80}(Sm_{0.17}Co_{0.83})_xFe_{20-x}$ ribbons is not observed. However, the magnetoresistive properties of $Cu_{80}Fe_{20}$ are enhanced and the MR amplitude is comparable to that observed in Cu–Fe–Co systems.

References

[1] Baibich M N, Broo J M and Fert A 1988 *Phys. Rev. Lett.* **61** 2472
[2] Berkowitz A E, Mitchell J R, Carey M J, Young A P and Zhang S 1992 *Phys. Rev. Lett.* **68** 3745
[3] Xiao J Q, Jiang J S and Chien C L 1992 *Phys. Rev. Lett.* **68** 3749
[4] Crisan O, Le Breton J M, Jianu A, Maignan A, Noguès M, Teillet J and Filoti G 2001 *J. Magn. Magn. Mater.* **234** 99
[5] Ding J, Eilon M, Street R, Smith P, McCormick P G and St Pierre T 1995 *J. Magn. Magn. Mater.* **140** 471
[6] Fultz B, Hamdeh H and Okamoto J 1990 *Hyperfine Interact.* **54** 799
[7] Majetich S A, Scott J H, Kirkpatrick E M, Chowdary K, Gallagher K and McHenry M E 1997 *Nanostruct. Mater.* **9** 291
[8] Papusoi C 1999 *J. Magn. Magn. Mater.* **195** 708
[9] Nagamine L C C M, Mevel B, Dieny B, Rodmacq B, Regnard J R, Revenant-Brizard C and Manzini I 1999 *J. Magn. Magn. Mater.* **195** 437
[10] Gregg J F, Thompson S M, Dawson S J, Ounadjela K, Staddon C R, Hamman J, Fermon C, Saux G and O'Grady K 1994 *Phys. Rev.* B **49** 1064
[11] Viegas A D C, Geshev J, Dorneles L S, Knobel M and Schmidt J E 1997 *J. Appl. Phys.* **82** 3047
[12] Allia P, Knobel M, Tiberto P and Vinai F 1995 *Phys. Rev.* B **52** 15398
[13] Ferrari E F, da Silva F C S and Knobel M 1997 *Phys. Rev.* B **56** 6086
[14] Miranda M G M, Bracho Rodriguez G J, Baibich M N, Ferrari E F, da Silva F C S and Knobel M 1998 *J. Magn. Magn. Mater.* **185** 331
[15] Zhang S and Levy P M 1994 *J. Appl. Phys.* **73** 5315
[16] Allia P, Coisson M, Durin G F, Moya J, Selvaggini V, Tiberto P and Vinai F 2002 *J. Appl. Phys.* **91** 5936
[17] Coisson M, Selvaggini V and Bosco E 2003 *J. Magn. Magn. Mater.* **262** 73
[18] Saxena S S, Tang J, Sooklee Y and O'Connor C 1994 *J. Appl. Phys.* **76** 16820
[19] Hihara T, Sumiyama K, Onodera H, Wakoh K and Suzuki K 1996 *Mater. Sci. Eng.* A **217/218** 322
[20] Rogalski M S, Pereia de Azevedo M M and Sousa J B 1996 *J. Magn. Magn. Mater.* **163** 257